NIFS--418
JP9611254

NATIONAL INSTITUTE FOR FUSION SCIENCE

Extraction of K^- Mesonlike Particles from a D_2 Gas Discharge Plasma in Magnetic Field

J. Uramoto

(Received - Oct. 24, 1995)

NIFS-418

May 1996

RESEARCH REPORT
NIFS Series

NAGOYA, JAPAN

Extraction of K^- mesonlike Particles from a D_2 gas Discharge Plasma in Magnetic Field

Jōshin URAMOTO

National Institute of Fusion Science,

Nagoya 464-01, Japan

Abstract

From the outside region of D_2 gas discharge plasma along magnetic field, K^- mesonlike particles are extracted with D^- ions and π^- mesonlike particles. Then, a higher positive bias voltage is necessary for the beam collector of magnetic mass analyzer in order to detect the K^- mesonlike particles, and we must interrupt the diffusion of the positive ions to the back of the beam collector.

Keywords: K^- mesonlike particle, D_2 gas discharge, D^- ion

It has been reported[1] already that negative pionlike particles (π^-) are extracted from the outside region of a H_2 or D_2 gas discharge plasma in magnetic field, together with H^- ions or D^- ions. However, physical differences between the H_2 and the D_2 gas discharge plasma were not investigated precisely under various experimental conditions. In this paper, a remarkable difference of extraction of negatively charged particles between a H_2 and D_2 gas discharge plasma will be clarified by adjusting a bias voltage of the beam collector of magnetic mass analyzer.

A schematic diagram of the experimental apparatus is shown in Fig. 1. The apparatus is constructed from a D_2 gas discharge plasma in magnetic fields, three extraction electrodes (with an aperture of 3 mm in diameter) to extract some negatively charged particles and a magnetic mass analyzer (90° deflection-type).

An electron acceleration-type sheet plasma[2] is produced to generate D^- ions effectively and in wide area. That is, the discharge (cylindrical) plasma flow of about 1 cm in diameter is transformed into a sheet plasma flow of about 3 mm in thickness and about 20 cm in width, while the electron components in the initial discharge plasma are accelerated near 80 eV. The sheet plasma flow passes through the electron acceleration anode (12 in Fig. 1) and enters the main chamber (50 cm long). The electron components in the sheet plasma are reflected by the end plate which is electrically floated. A uniform magnetic field of about 50 gauss is applied along the sheet plasma flow in the main chamber where the D_2 gas pressure is about 1.5×10^{-3} Torr. The electron acceleration anode current I_A is 30A and about 60% of I_A enters the main chamber. A distance between the sheet plasma center and the first extraction electrode (L) is 7.5 cm. The plasma density in the center of the sheet plasma is about 10^{11}/cc and the electron temperature is about 20 eV. The positive ion density in front of the first extraction electrode is estimated to be about 10^{10}/cc from a positive ion saturation current as D_3^+, while the electron density from the Langmuir probe characteristic is about 10^9/cc and the electron temperature is about 3.0 eV. That is, the electron density in front of the first extraction electrode is reduced near 1/10 of the positive ion density.

The negatively charged particles extracted from the D_2 gas discharge plasma, are injected into the ordinary magnetic mass analyzer (MA) through the slit (3 mm × 1 cm) while each mass of the negatively charged particle is estimated by the following relations: From the analyzing magnetic field B_M where the negative current to the beam collector BC shows a peak, the curvature radius r

of the mass analyzer and the extraction (acceleration) voltage V_E, we can estimate the mass m of the negatively charged particle by,

$$m = \frac{Ze\,(B_M r)^2}{2V_E}$$

$$= \frac{8.8 \times 10^{-2}\, Z\,(B_M r)^2\, m_e}{V_E}, \quad \text{..... (1)}$$

where e is the electron charge, B_M is in gauss unit, r is in cm unit, V_E is in volt unit and m_e is the electron mass and Z is the charge number. For the curvature radius $r = 4.3$ cm of this mass analyzer, the Eq. (1) is rewritten by

$$m = \frac{1.63\, Z\, B_M^2}{V_E} m_e. \quad \text{..... (2)}$$

In the extraction of negatively charged particles, the first extraction electrode (L) is electrically floated, whose potential V_L is about −15V with respect to the electron acceleration anode (12 in Fig. 1). A potential V_M of the second extraction electrode (M) is kept at 300V. The potential V_E of the final extraction electrode (E) is 800V.

A result of the mass analysis for extraction of negatively charged particles from the D_2 gas discharge plasma, is shown in Fig. 2. Dependences of the negative current I^- to the beam collector on the analyzing magnetic field B_M are shown, where the bias voltage V_{BC} of the beam collector with respect to the mass analyzer, is 50V or 140V.

For $V_{BC} = 50$V [(1) of Fig. 2], the first peak of negative current I^- to the beam collector is seen at $B_M \approx 390$ gauss while the second peak appears at $B_M \approx 1420$ gauss. From Eq. (2), we obtain $m_1 \approx 310\, m_e$ and $m_2 \approx 4100\, m_e$, assuming that $Z = 1$. On the other hand, for $V_{BC} = 140$V [(2) for Fig. 2], the third peak appears at $B_M \approx 720$ gauss between the first peak and the second peak, which corresponds to $m_3 \approx 1050\, m_e$, assuming that $Z = 1$.

For the above experimental results of Fig. 2, we can estimate that the first particle mass (m_1) is near the typical negative pion π^- mass (= 273 m_e) within 14% and the second particle mass (m_2) is near D^- ion mass (= 3680 m_e) within 12%. Here, we find that the third particle mass (m_3) is near the typical K^- meson mass (= 966 m_e) within 9%, assuming that $Z = 1$ also.

In the experiment of Fig. 3, a Cu plate of 0.5 mm in thickness is put in front of the beam collector of the mass analyzer. Then, the second current peak corresponding to D^- ion disappears while the first and the third current peak appear. This experimental fact shows that the pionlike particle π^- and the K^- mesonlike particle penetrate the Cu plate. It has been reported[3] already that the pionlike π^- or muonlike particle μ^- penetrates a metal plate if the positive ions exist behind the metal plate. In this experiment, those positive ions may be produced by the gas ionization due to D^- ions. From these experimental results, we find that a physical character of the first peak particle (π^-) and the third peak particle (K^-) is remarkably different from that of the second peak particle (D^-).

Next, in order to clarify differences for the third peak (K^-) between a D_2 gas and H_2 gas discharge plasma, extractions of negatively charged particles from a H_2 gas discharge plasma are tried under experimental conditions similar to the D_2 gas discharge plasma (that is, $B_Z \approx 50$ gauss, $I_A = 30A$, $V_M = 300V$ and $P \approx 1.5 \times 10^{-3}$ Torr of H_2 gas). The experimental results for the H_2 gas discharge plasma are shown in Fig. 4 (in the ordinary method) and in Fig. 5 (in the "Cu plate arrangement" method). In Fig. 4, the first current peak (corresponding to π^-) and the second current peak (H^-) are seen under the beam collector bias voltage $V_{BC} = 50V$ and $V_{BC} = 140V$. In Fig. 5, only the first current peak (π^-) is seen. As understood from these experimental results, the third current peak corresponding to the K^- mesonlike particle does not appear for H_2 gas discharge plasmas. We have confirmed that the K^- mesonlike particles are not extracted from H_2 gas discharge plasmas even if the experimental conditions are varied greatly.

A dependence of the K^- mesonlike current peak to the beam collector on the extraction voltage V_E is investigated from 700V to 1200V, which satisfys Eq (2). The K^- mesonlike current peak does not appear for $V_E < 700V$ while the π^- current peak does not appear for $V_E < 400V$. That reason may be due to the life time ($\approx 1.2 \times 10^{-8}$ sec) of K^- meson which is shorter than that of π^- meson ($\approx 2.6 \times 10^{-8}$ sec).

In conclusion, the K^- mesonlike particles generate as some physical differences between the H_2 gas and D_2 gas discharge plasma. A higher positive bias voltage of the beam collector is necessary to detect the K^- mesonlike particles and we must interrupt the diffusion of the positive ions to the back of the beam collector [4] (Fig. 2 MA).

References

1) J. Uramoto: National Institute of Fusion Science, Nagoya, Japan-Research Report, NIFS-377 (1995).

2) J. Uramoto: Journal of the vacuum society of Japan, **37** (1994) 507 in Japanese.

3) J. Uramoto: NIFS-350 (1995).

4) J. Uramoto: NIFS-400(1996).

Figure Captions

Fig. 1 Schematic diagram of experimental apparatus.

1: Cylindrical plasma in discharge anode. 2: Discharge cathode. 3: D_2 gas flow. 4: Discharge power supply. 5: Electron acceleration power supply. 6: Vacuum pump. 7: Area where cylindrical plasma is transformed into sheet plasma. 8: Insulation tube. 9: A pair of permanent magnets. 10: Magnetic field coils. 11: slit of acceleration anode. 12: Electron acceleration anode. 13: Floated end electrode. I_A: Current to electron acceleration anode. CP: Cylindrical plasma. SP: Sheet plasma. B_Z: Magnetic field. L: First extraction electrode. M: Second extraction electrode. E: Final extraction electrode. V_M: Potential (300V) of second extraction electrode with respect to electron acceleration anode. V_E: Potential (800V) of final extraction electrode with respect to electron acceleration anode. I_E: Negative current to final extraction electrode. MA: Magnetic deflection (90°) mass analyzer. B_M: Magnetic field intensity of MA. BC: Beam collector of MA. V_{BC}: Positive potential of BC with respect to MA. Γ^-: Negative current to BC. I_{MA}: Total negative current to MA. $D_{\bar{0}}$: Deuteron negative ions outside of sheet plasma. D^-: Accelerated deuteron negative ions. $\pi_{\bar{0}}$: Negative pionlike particles outside of sheet plasma. π^-: Accelerated negative pionlike particles. $K_{\bar{0}}$: K^- mesonlike particles outside of sheet plasma.

Fig. 2 Dependences of negative current Γ^- to beam collector on magnetic field intensity B_M of MA at V_E = 800V. (1): V_{BC} = 50V. (2): V_{BC} = 140V.

π^-: First peak of Γ^- corresponding to negative pionlike particle. D^-: Second peak of Γ^- corresponding to deuteron negative ion. K^- : Third peak of Γ^- corresponding to K^- mesonlike particle.

Fig. 3 Dependences of negative current Γ^- on B_M under a case setting a Cu plate in front of beam collector at V_E = 800V. π^-: First peak of Γ^-. K^-: Third peak of Γ^-. (D^-): Position of second peak of Γ^-. Cu: Copper plate of 0.5 mm in thickness, which shields the surface of beam collector. (1): V_{BC} = 50V. (2): V_{BC} = 140V.

Fig. 4 Dependences (for H_2 gas) of negative current Γ^- on B_M at V_E = 800V.

(1): V_{BC} = 50. (2): V_{BC} = 140V. π^-: First peak of Γ^-. H^-: Second peak of Γ^- corresponding to hydrogen negative ion.

Fig. 5 Dependences (for H_2 gas) of negative current I^- on B_M under a case setting a Cu plate in front of beam collector at $V_E = 800V$.

(1): $V_{BC} = 50V$. (2): $V_{BC} = 140V$. π^-: First peak of I^-.

Appendix

Schematic diagrams of the magnetic mass analyzer and the extraction electrodes are shown in Fig. 1 MA and Fig. 2 MA. The (fringe) magnetic field distribution is shown in Fig. 3 MA also.

Figure Captions of Appendix

Fig. 1 MA and Fig. 2 MA Schematic diagrams of mass analyzer M.A. and the extraction electrodes E.M.L.

E: final extraction electrode (with an aperture of 3 mm in diameter). V_E: Applied voltage of E. I_E: Negative current to E. S: Entrance slit (3 mm × 10 mm) of M.A. Fe: shows Iron. C: Magnetic coil. (N): North pole of electro-magnet. (S): South pole. B_M: Analyzing magnetic field. B.C: Beam collector. I^-: Negative current to B.C. V_{BC}: Bias voltage of B.C. with respect to M.A. X: Entrance of uniform magnetic field. H^-: Hydrogen negative ion. D^-: Deuteron negative ion. π^-: Negative pionlike particle. K^-: K^- mesonlike particle. Ins: Insulator.

Fig. 3 MA Fringe magnetic field distribution at (1A of M.A. coil current).

B_M: Analyzing magnetic field of M.A. B_0: Uniform magnetic field inside of M.A. S: Entrance slit position. X: End of uniform magnetic field.

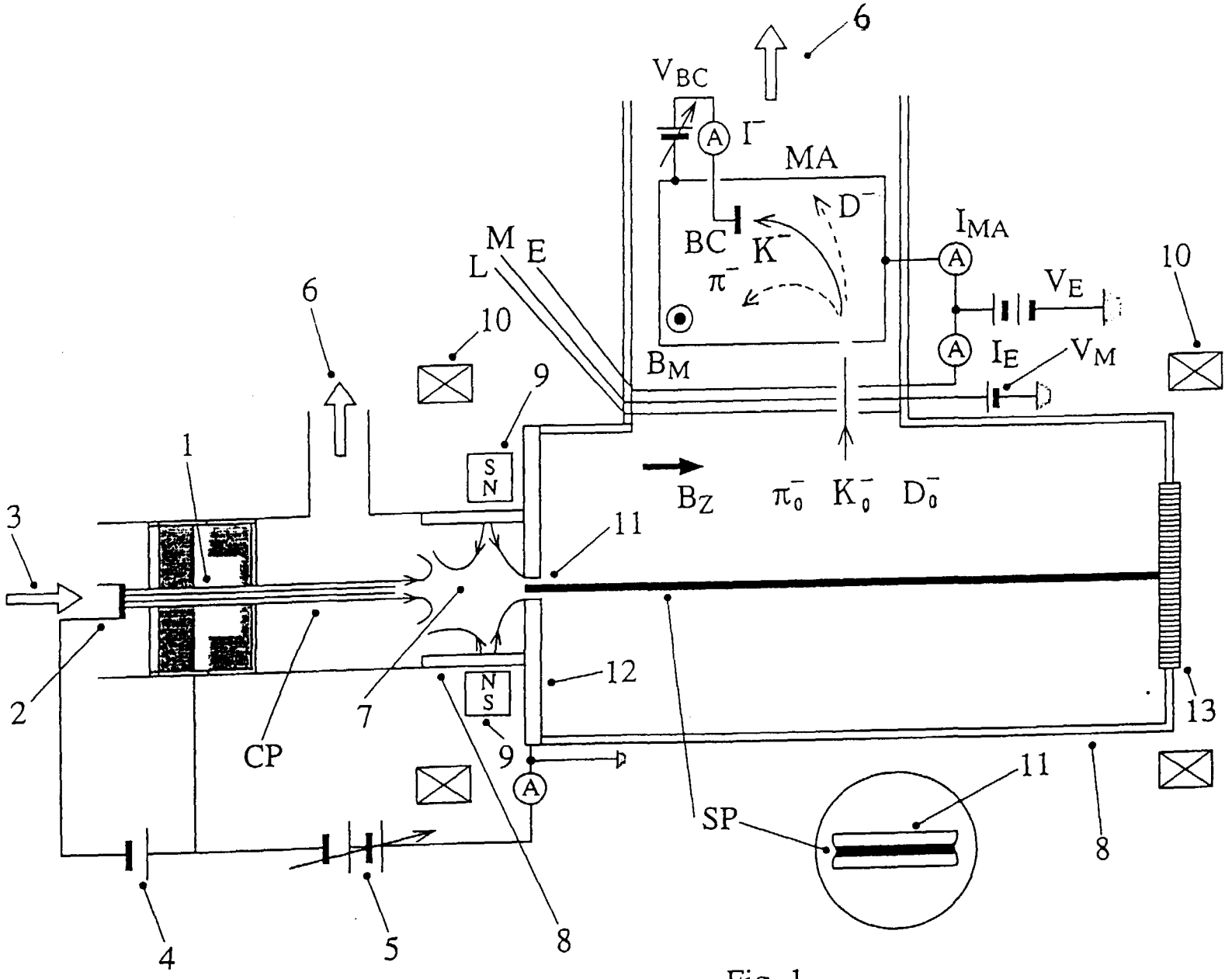
6
V_{BC}
A
I^-
MA
D^-
BC
K^-
π^-
I_{MA}
M
L
E
10
V_E
I_E
V_M
B_M
9
1
B_Z
π_0^-
K_0^-
D_0^-
3
11
2
CP
7
12
13
N
S
9
SP
11
8
4
5
8

Fig. 1

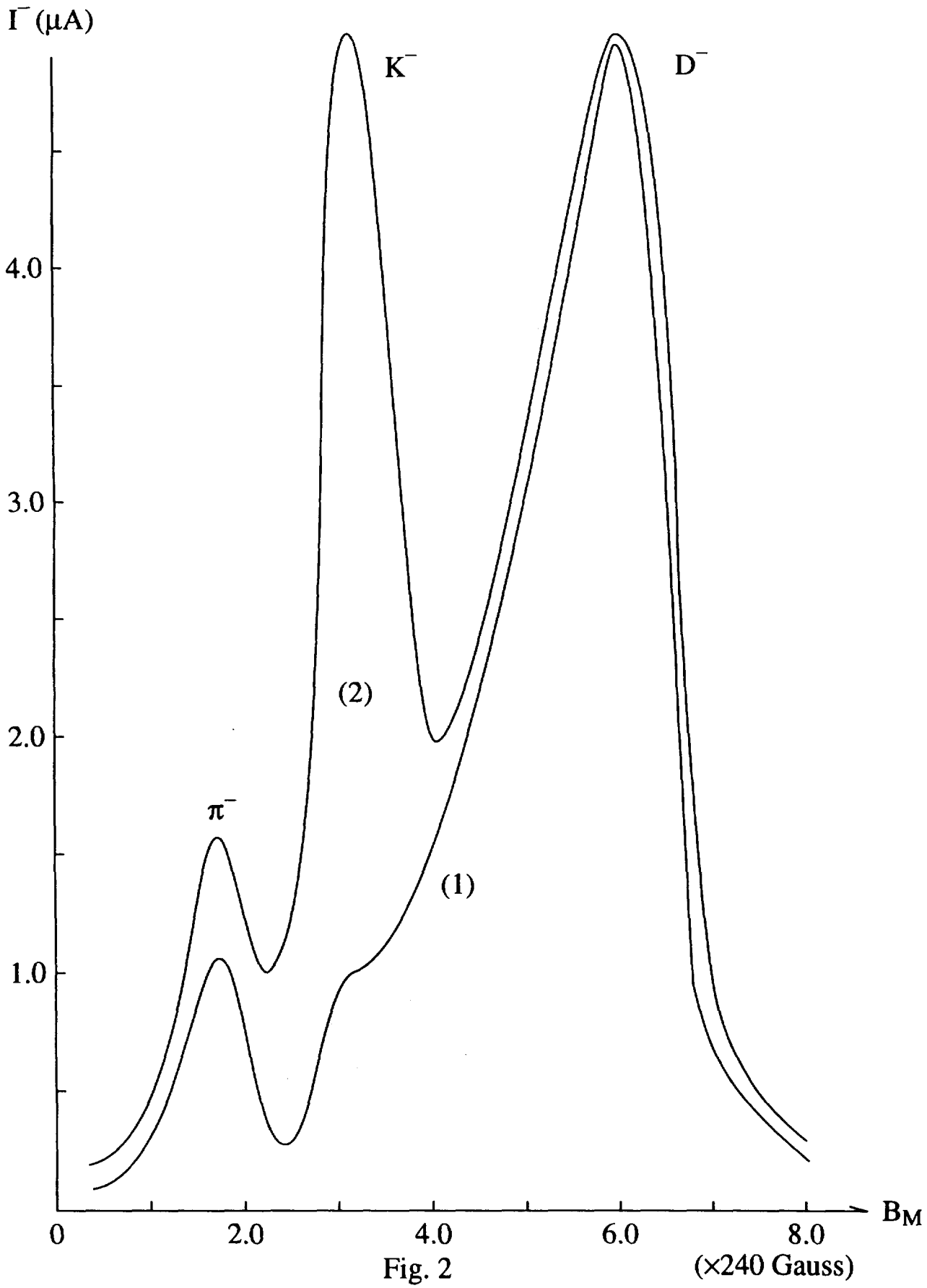

Fig. 2

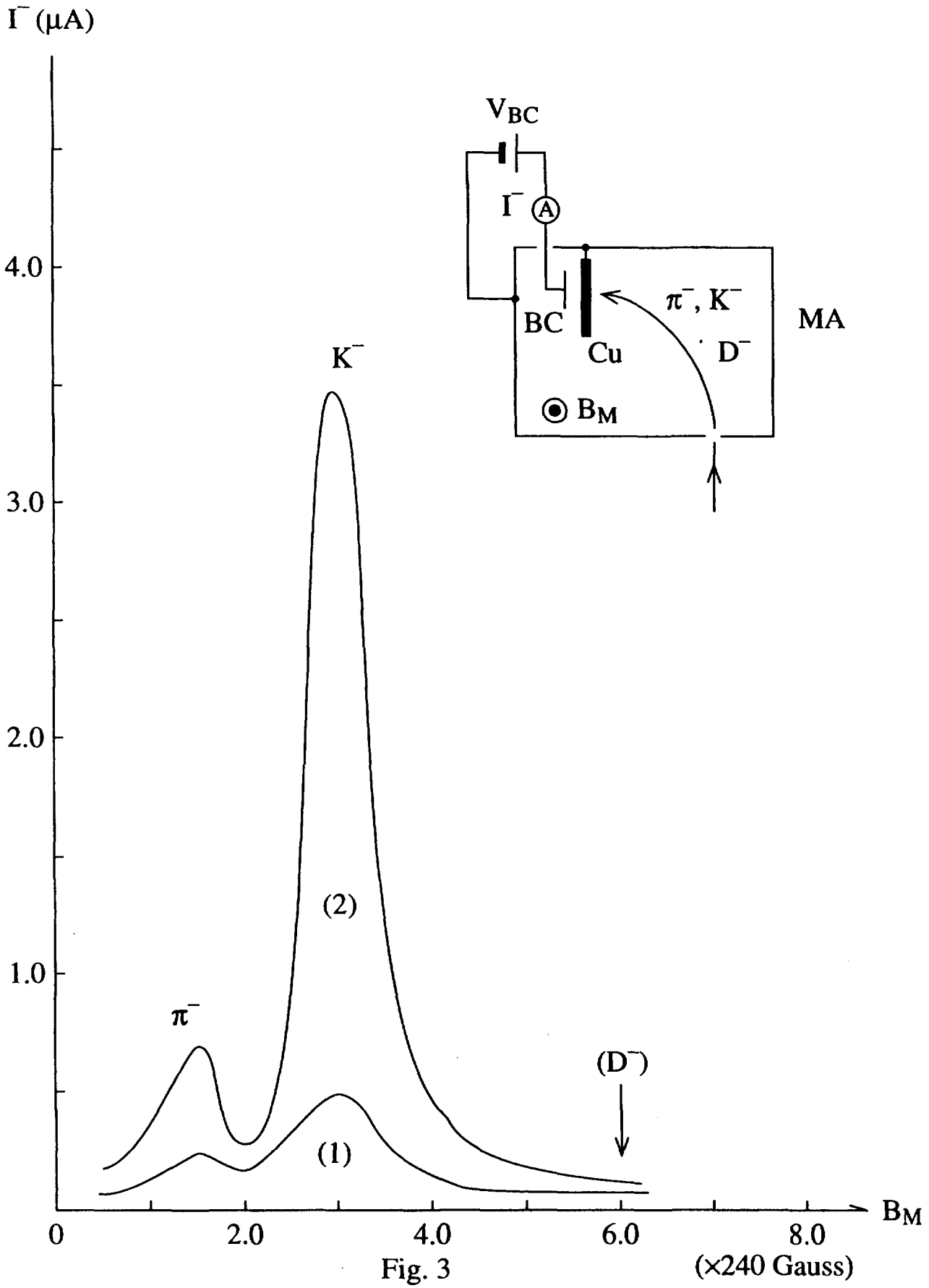
I⁻ (μA)
4.0
3.0
2.0
1.0
0
2.0
4.0
6.0
8.0
(×240 Gauss)
B_M
K⁻
π⁻
(D⁻)
(1)
(2)
V_BC
I⁻
A
BC
Cu
π⁻, K⁻
D⁻
MA
B_M

Fig. 3

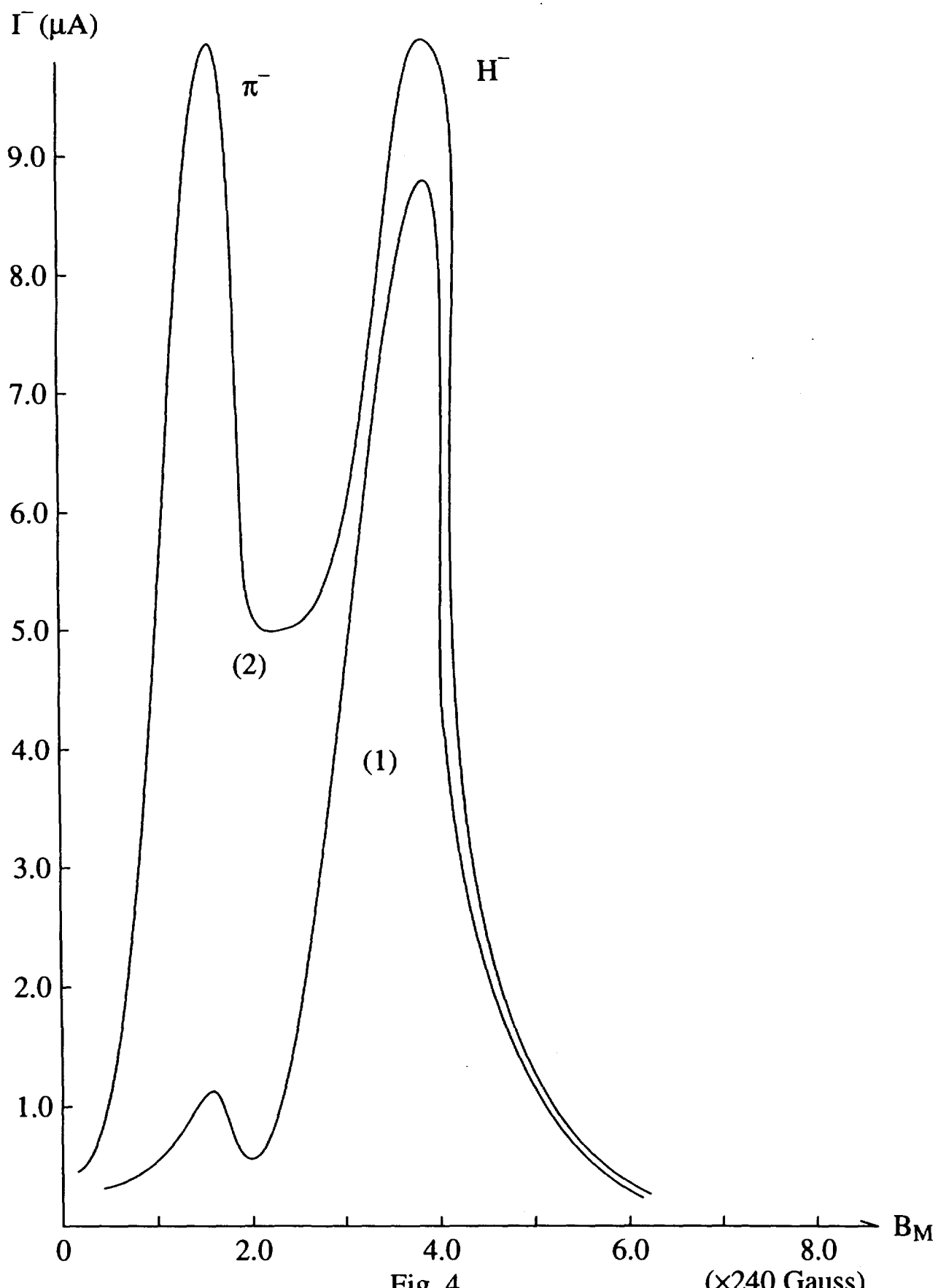

Fig. 4

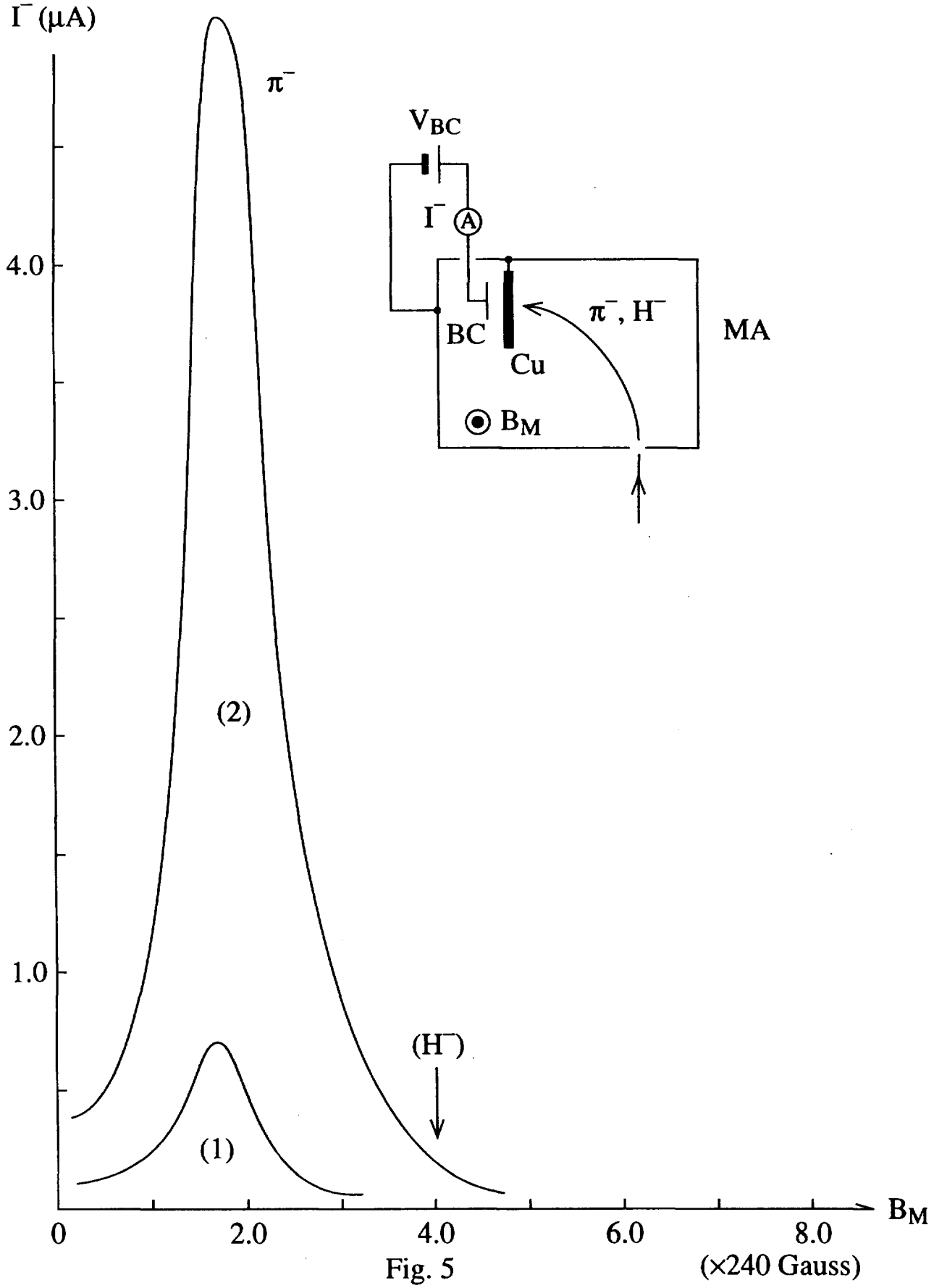

Fig. 5

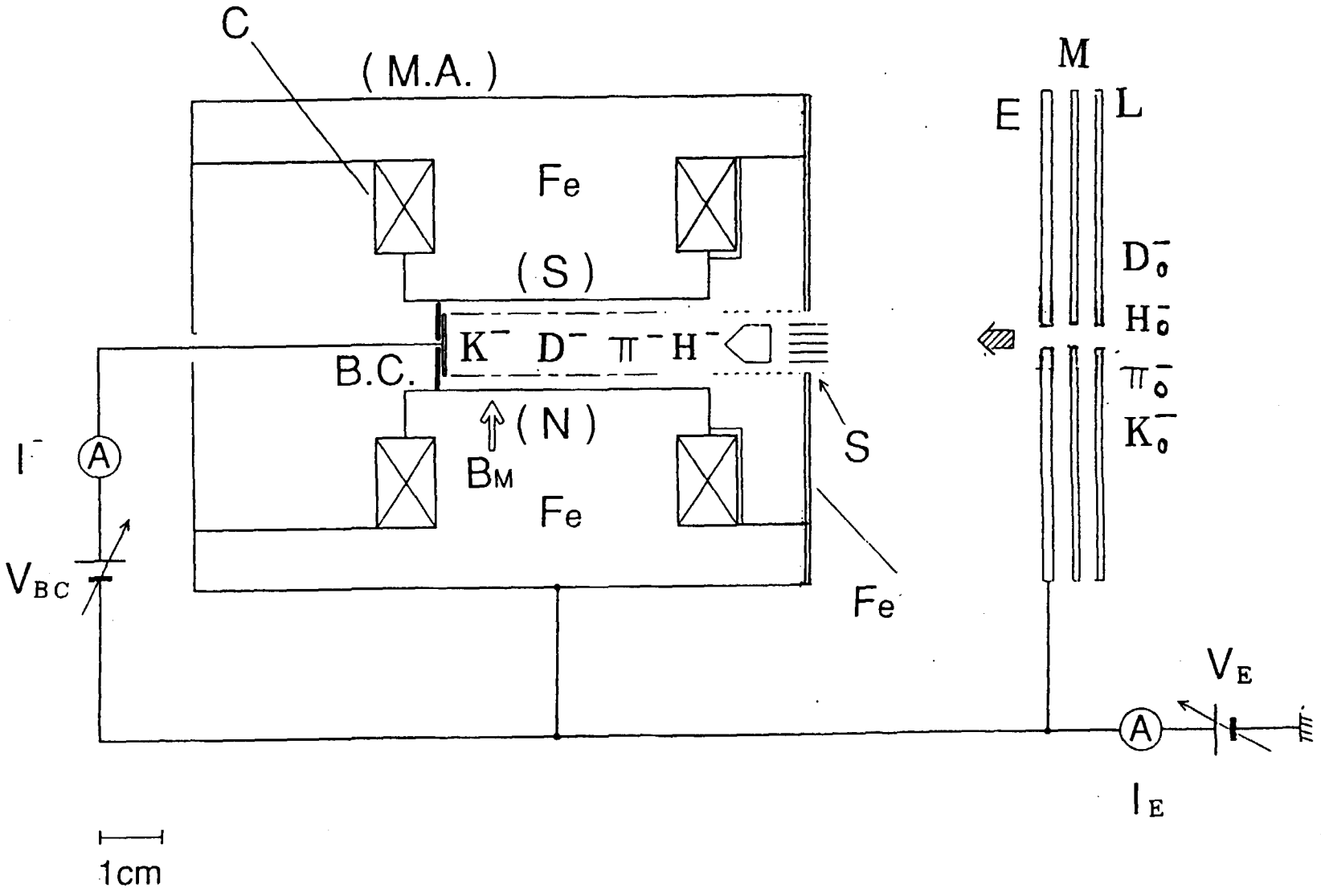

Fig. 1 MA

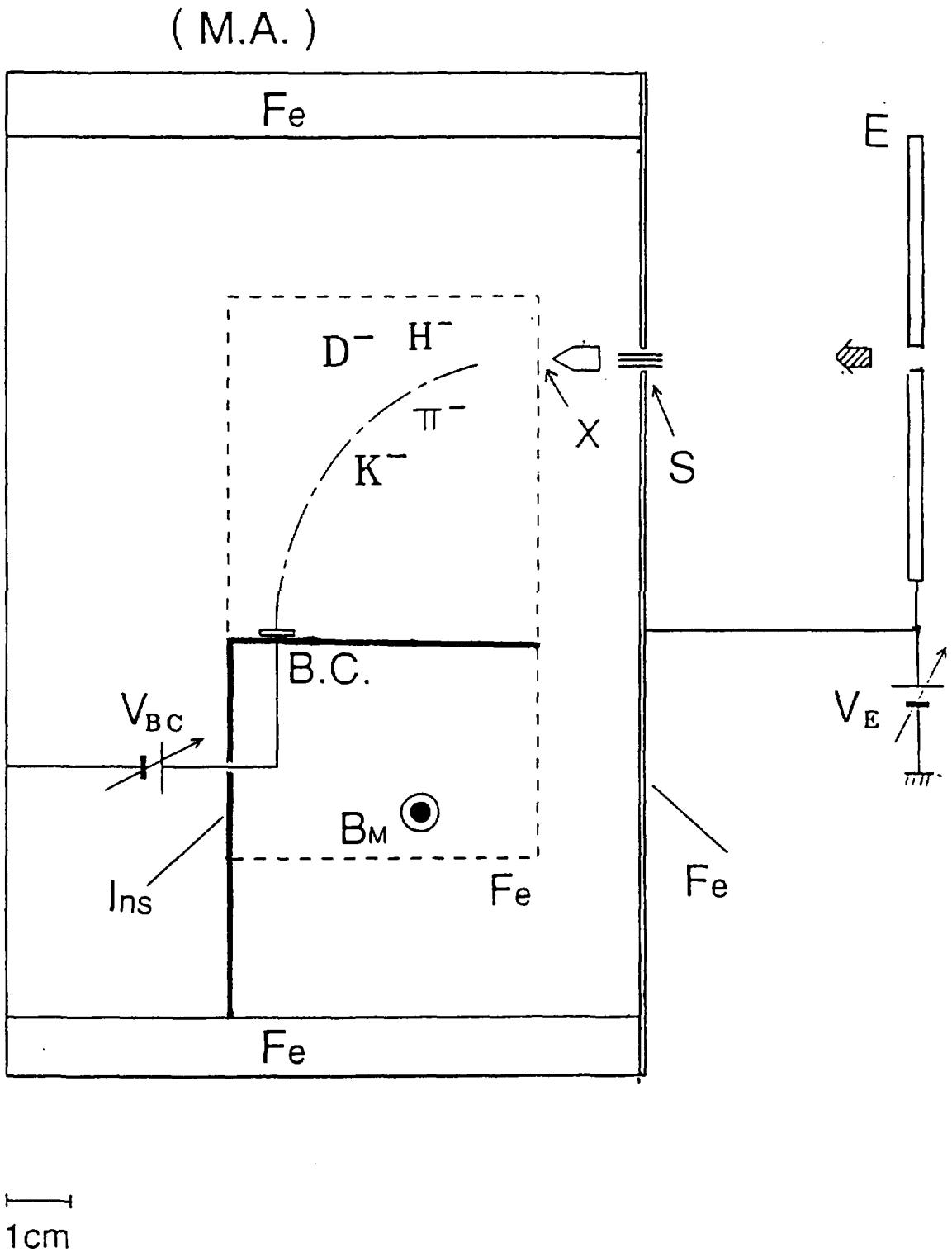

Fig. 2 MA

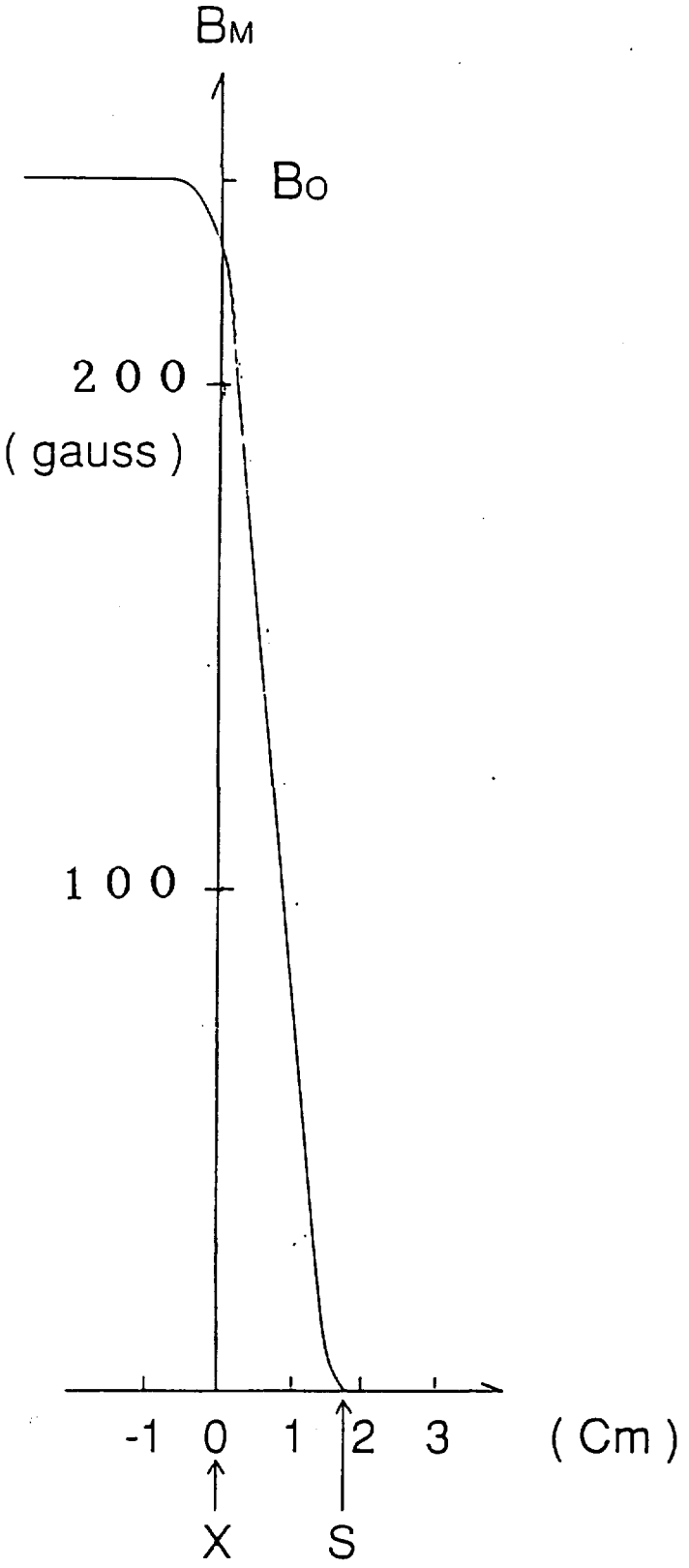

Fig. 3 MA

Recent Issues of NIFS Series

NIFS-371 S. Yamaguchi, J. Yamamoto and O. Motojima;
A New Cable -in conduit Conductor Magnet with Insulated Strands; Sep. 1995

NIFS-372 H. Miura,
Enstrophy Generation in a Shock-Dominated Turbulence; Sep. 1995

NIFS-373 M. Natsir, A. Sagara, K. Tsuzuki, B. Tsuchiya, Y. Hasegawa, O. Motojima,
Control of Discharge Conditions to Reduce Hydrogen Content in Low Z Films Produced with DC Glow; Sep. 1995

NIFS-374 K. Tsuzuki, M. Natsir, N. Inoue, A. Sagara, N. Noda, O. Motojima, T. Mochizuki, I. Fujita, T. Hino and T. Yamashina,
Behavior of Hydrogen Atoms in Boron Films during H_2 and He Glow Discharge and Thermal Desorption; Sep. 1995

NIFS-375 U. Stroth, M. Murakami, R.A. Dory, H. Yamada, S. Okamura, F. Sano and T. Obiki,
Energy Confinement Scaling from the International Stellarator Database; Sep. 1995

NIFS-376 S. Bazdenkov, T. Sato, K. Watanabe and The Complexity Simulation Group,
Multi-Scale Semi-Ideal Magnetohydrodynamics of a Tokamak Plasma; Sep. 1995

NIFS-377 J. Uramoto,
Extraction of Negative Pionlike Particles from a H2 or D2 Gas Discharge Plasma in Magnetic Field; Sep. 1995

NIFS-378 K. Akaishi,
Theoretical Consideration for the Outgassing Characteristics of an Unbaked Vacuum System; Oct. 1995

NIFS-379 H. Shimazu, S. Machida and M. Tanaka,
Macro-Particle Simulation of Collisionless Parallel Shocks; Oct. 1995

NIFS-380 N. Kondo and Y. Kondoh,
Eigenfunction Spectrum Analysis for Self-organization in Dissipative Solitons; Oct. 1995

NIFS-381 Y. Kondoh, M. Yoshizawa, A. Nakano and T. Yabe,
Self-organization of Two-dimensional Incompressible Viscous Flow in a Friction-free Box; Oct. 1995

NIFS-382 Y.N. Nejoh and H. Sanuki,
The Effects of the Beam and Ion Temperatures on Ion-Acoustic Waves in an

Electron Beam-Plasma System; Oct. 1995

NIFS-383 K. Ichiguchi, O. Motojima, K. Yamazaki, N. Nakajima and M. Okamoto
Flexibility of LHD Configuration with Multi-Layer Helical Coils;
Nov. 1995

NIFS-384 D. Biskamp, E. Schwarz and J.F. Drake,
Two-dimensional Electron Magnetohydrodynamic Turbulence; Nov. 1995

NIFS-385 H. Kitabata, T. Hayashi, T. Sato and Complexity Simulation Group,
Impulsive Nature in Collisional Driven Reconnection; Nov. 1995

NIFS-386 Y. Katoh, T. Muroga, A. Kohyama, R.E. Stoller, C. Namba and O. Motojima,
Rate Theory Modeling of Defect Evolution under Cascade Damage Conditions:The Influence of Vacancy-type Cascade Remnants and Application to the Defect Production Chracterization by Microstructural Analysis; Nov. 1995

NIFS-387 K. Araki, S. Yanase and J. Mizushima,
Symmetry Breaking by Differential Rotation and Saddle-node Bifurcation of the Thermal Convection in a Spherical Shell; Dec. 1995

NIFS-388 V.D. Pustovitov,
Control of Pfirsch-Schlüter Current by External Poloidal Magnetic Field in Conventional Stellarators: Dec. 1995

NIFS-389 K. Akaishi,
On the Outgassing Rate Versus Time Characteristics in the Pump-down of an Unbaked Vacuum System; Dec. 1995

NIFS-390 K.N. Sato, S. Murakami, N. Nakajima, K. Itoh,
Possibility of Simulation Experiments for Fast Particle Physics in Large Helical Device (LHD); Dec. 1995

NIFS-391 W.X.Wang, M. Okamoto, N. Nakajima, S. Murakami and N. Ohyabu,
A Monte Carlo Simulation Model for the Steady-State Plasma in the Scrape-off Layer; Dec. 1995

NIFS-392 Shao-ping Zhu, R. Horiuchi, T. Sato and The Complexity Simulation Group,
Self-organization Process of a Magnetohydrodynamic Plasma in the Presence of Thermal Conduction; Dec. 1995

NIFS-393 M. Ozaki, T. Sato, R. Horiuchi and the Complexity Simulation Group
Electromagnetic Instability and Anomalous Resistivity in a Magnetic Neutral Sheet; Dec. 1995

NIFS-394 K. Itoh, S.-I Itoh, M. Yagi and A. Fukuyama,
Subcritical Excitation of Plasma Turbulence; Jan. 1996

NIFS-395 H. Sugama and M. Okamoto, W. Horton and M. Wakatani,
Transport Processes and Entropy Production in Toroidal Plasmas with Gyrokinetic Eletromagnetic Turbulence; Jan. 1996

NIFS-396 T. Kato, T. Fujiwara and Y. Hanaoka,
X-ray Spectral Analysis of Yohkoh BCS Data on Sep. 6 1992 Flares - Blue Shift Component and Ion Abundances -; Feb. 1996

NIFS-397 H. Kuramoto, N. Hiraki, S. Moriyama, K. Toi, K. Sato, K. Narihara, A. Ejiri, T. Seki and JIPP T-IIU Group,
Measurement of the Poloidal Magnetic Field Profile with High Time Resolution Zeeman Polarimeter in the JIPP T-IIU Tokamak; Feb. 1996

NIFS-398 J.F. Wang, T. Amano, Y. Ogawa, N. Inoue,
Simulation of Burning Plasma Dynamics in ITER; Feb. 1996

NIFS-399 K. Itoh, S-I. Itoh, A. Fukuyama and M. Yagi,
Theory of Self-Sustained Turbulence in Confined Plasmas; Feb. 1996

NIFS-400 J. Uramoto,
A Detection Method of Negative Pionlike Particles from a H2 Gas Descharge Plasma; Feb. 1996

NIFS-401 K.Ida, J.Xu, K.N.Sato, H.Sakakita and JIPP TII-U group,
Fast Charge Exchange Spectroscopy Using a Fabry-Perot Spectrometer in the JIPP TII-U Tokamak; Feb. 1996

NIFS-402 T. Amano,
Passive Shut-Down of ITER Plasma by Be Evaporation; Feb. 1996

NIFS-403 K. Orito,
A New Variable Transformation Technique for the Nonlinear Drift Vortex; Feb. 1996

NIFS-404 T. Oike, K. Kitachi, S. Ohdachi, K. Toi, S. Sakakibara, S. Morita, T. Morisaki, H. Suzuki, S. Okamura, K. Matsuoka and CHS group; *Measurement of Magnetic Field Fluctuations near Plasma Edge with Movable Magnetic Probe Array in the CHS Heliotron/Torsatron*; Mar. 1996

NIFS-405 S.K. Guharay, K. Tsumori, M. Hamabe, Y. Takeiri, O. Kaneko, T. Kuroda,
Simple Emittance Measurement of H- Beams from a Large Plasma Source; Mar. 1996

NIFS-406 M. Tanaka and D. Biskamp,
Symmetry-Breaking due to Parallel Electron Motion and Resultant Scaling in Collisionless Magnetic Reconnection; Mar. 1996

NIFS-407 K. Kitachi, T. Oike, S. Ohdachi, K. Toi, R. Akiyama, A. Ejiri, Y. Hamada,

H.Kuramoto, K. Narihara, T. Seki and JIPP T-IIU Group,
Measurement of Magnetic Field Fluctuations within Last Closed Flux Surface with Movable Magnetic Probe Array in the JIPP T-IIU Tokamak; Mar. 1996

NIFS-408 K. Hirose, S. Saito and Yoshi.H. Ichikawa
Structure of Period-2 Step-1 Accelerator Island in Area Preserving Maps; Mar. 1996

NIFS-409 G.Y.Yu, M. Okamoto, H. Sanuki, T. Amano,
Effect of Plasma Inertia on Vertical Displacement Instability in Tokamaks; Mar. 1996

NIFS-410 T. Yamagishi,
Solution of Initial Value Problem of Gyro-Kinetic Equation; Mar. 1996

NIFS-411 K. Ida and N. Nakajima,
Comparison of Parallel Viscosity with Neoclassical Theory; Apr. 1996

NIFS-412 T. Ohkawa and H. Ohkawa,
Cuspher, A Combined Confinement System; Apr. 1996

NIFS-413 Y. Nomura, Y.H. Ichikawa and A.T. Filippov,
Stochasticity in the Josephson Map; Apr. 1996

NIFS-414 J. Uramoto,
Production Mechanism of Negative Pionlike Particles in H_2 Gas Discharge Plasma; Apr. 1996

NIFS-415 A. Fujisawa, H. Iguchi, S. Lee, T.P. Crowley, Y. Hamada, S. Hidekuma, M. Kojima,
Active Trajectory Control for a Heavy Ion Beam Probe on the Compact Helical System; May 1996

NIFS-416 M. Iwase, K. Ohkubo, S. Kubo and H. Idei
Band Rejection Filter for Measurement of Electron Cyclotron Emission during Electron Cyclotron Heating; May 1996

NIFS-417 T. Yabe, H. Daido,T. Aoki, E. Matsunaga and K. Arisawa,
Anomalous Crater Formation in Pulsed-Laser-Illuminated Aluminum Slab and Debris Distribution; May 1996

NIFS-418 J. Uramoto,
Extraction of K^- Mesonlike Particles from a D_2 Gas Discharge Plasma in Magnetic Field; May 1996